General Muscle Torque Generator Model for a Two Degree-of-Freedom Shoulder Joint

Sydney Bell[1]
Systems Design Engineering Department,
University of Waterloo,
Waterloo, ON, Canada.
email: sm3bell@uwaterloo.ca

Ali Nasr
Postdoctoral Research Associate,
Systems Design Engineering Department,
University of Waterloo,
Waterloo, ON, Canada.
email: a.nasr@uwaterloo.ca

John McPhee
Professor and Canada Research Chair,
Systems Design Engineering Department,
University of Waterloo,
Waterloo, ON, Canada.
email: mcphee@uwaterloo.ca

Muscle Torque Generators (MTGs) have been developed as an alternative to muscle-force models, reducing the muscle-force model complexity to a single torque at the joint. Current MTGs can only be applied to single Degree-of-Freedom (DoF) joints, leading to complications in modeling joints with multiple-DoFs such as the shoulder. This study aimed to develop an MTG model that accounts for the coupling between 2-DoF at the shoulder joint: shoulder plane of elevation (horizontal abduction/adduction) and shoulder elevation (flexion/extension). Three different 2-DoF MTG equations were developed to model the coupling between these two movements. Net joint torques at the shoulder were determined for 20 participants (10 females and 10 males) in isometric, isokinetic, and passive tests. Curve and surface polynomial fitting was used to find the best general fit for the experimental data in terms of the different degrees of coupling. The models were validated against experimental isokinetic torque data. It was determined that implicit coupling that used interpolation between single-DoF MTGs resulted in the lowest root mean square percent error of 8.5%. The work demonstrated that general MTG models can predict torque results that are dependent on multiple-DoFs of the shoulder.

Keywords: muscle torque generator, shoulder joint, torque-angle relationship, torque-velocity relationship, muscle mechanics

1 Introduction

Musculoskeletal models are integral to biomechanics simulations across diverse domains, as evidenced by their application in predictive biomechanics simulation [1], the formulation and evaluation of effective rehabilitation strategies [2], the design and control of wearable robots [3,4], and the optimization of motions or tools for sports applications [5–7]. To create a human musculoskeletal model for simulations, a reasonable representation of muscles is required, and Hill-type muscle-force models are often applied [1,8]. However, these muscle-force models have some drawbacks, including the need to define muscle geometry such as the insertion point, wrapping, and the muscle moment arm [9–12]. There is also the muscle redundancy issue, in which there are more muscles crossing a joint than Degrees of Freedom (DoFs), requiring optimization to solve for unique muscle forces [11–13]. Finally, these muscle-force models require parameters that can be difficult to identify [11,12,14]. One solution to the mentioned drawbacks is to use a Muscle Torque Generator (MTG) as it reduces the complexity of muscle-force models to a single torque at the joint, all while maintaining the position and velocity dependencies of muscles [11,14,15].

The standard form of an MTG model is a functional equation containing a torque-angle scaling function, τ_θ, which represents the length-dependent properties of muscles, a torque-velocity scaling function, τ_ω, which represents the muscle lengthening-dependent properties, a passive function, τ_p, which considers forces from viscoelastic elements of the muscle, and finally the activation function, τ_{act}, which gives active torque [11,12,14,15]. The functional equation in Equation (1) is the standard form of a single-DoF MTG for joint angle θ and angular velocity ω.

$$\tau(\tau_{act}, \theta, \omega) = \tau_{act} \cdot \tau_\omega(\omega) \cdot \tau_\theta(\theta) + \tau_p(\theta, \omega) \tag{1}$$

The four crucial sub-functions, the torque-angle scaling, the torque-velocity scaling, the passive, and the activation models are thoroughly introduced in the subsequent paragraphs.

The torque-angle scaling function τ_θ scales the maximum isometric torque such that the length-dependent properties of muscles are incorporated. Kulig et al [16] conducted work to determine human strength curves, which are curves that outline the torque-angle relationship of a joint. The authors found that a similar trend could be seen between the torque-angle curve of a joint and the force-length curve of muscles. In a typical force-length strength curve, a peak in muscle strength is achieved when the sarcomere length is optimal, and zero force is seen at the smallest and longest lengths [17]. Previous mathematical models of the force-length curves of muscles can therefore be used as inspiration for the torque-angle scaling function. The torque-angle scaling function has previously been modeled using a normal function [18], cosine [5,18,19], quadratic [18,20], cubic [18], and sine-exponential [18].

The torque-velocity scaling function τ_ω scales the maximum isometric torque production such that the lengthening properties of muscles are considered. During concentric motion, an increase in the speed of muscle shortening causes the muscle force to decrease in a hyperbolic nature [8]. However, in the eccentric phase, it has been found that maximum muscle force will increase to a value of 1.5 times the isometric force, with a plateau at higher speeds [21]. The function commonly employs a double hyperbolic model of the torque-velocity relationship [7,18,19,22,23], often utilizing a piecewise function to capture concentric and eccentric relationships [7,19,23].

The passive function allows for torques contributed by components in parallel with the contractile elements of muscle to be considered. These include structures such as tendons, ligaments and muscle tissues such as the epimysium and perimysium [14,19]. For passive function τ_p, two main forms exist: a double-exponential [12,19,24–26] and a linear spring-damper form [27,28].

Finally, the activation function τ_{act} captures the activation of muscles and provides a torque between the minimum isometric torque and the maximum isometric torque. The function is modeled using two main strategies: a function to capture the muscle activation dynamics [6,7,12,23], and a time-varying activation, a, that is bounded between 0 and 1 [5,12,15,20].

Previous studies have been conducted to determine how to best represent joint scaling relationships, with dynamometry often used to determine parameters for the evaluated joint [18–20,22,23,29].

Currently MTGs are used for single-DoF joints and additional MTGs are often added to represent joints with multiple-DoFs [6]. A biarticular approach has been implemented that incorporates the

[1]Corresponding Author.
Version 1.18, March 21, 2024

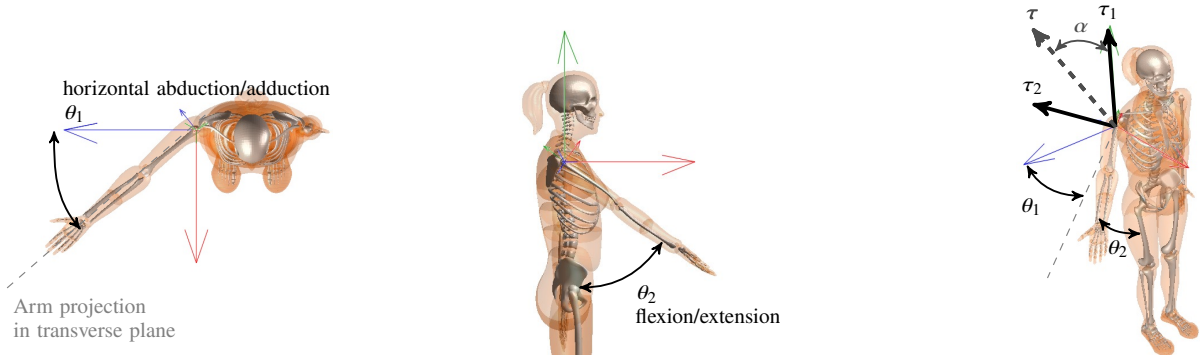

(a) Transverse plane view
$\theta_1 = 30°$ and $\theta_2 = 90°$

(b) Sagittal plane view
$\theta_1 = 90°$ and $\theta_2 = 45°$

(c) Three-dimensional view
$\theta_1 = 30°$ and $\theta_2 = 60°$

Fig. 1 Illustration of angle directions and torque examples for shoulder plane of elevation (horizontal abduction/adduction) and shoulder elevation (flexion/extension) for (a) Transverse plane view, (b) Sagittal plane view, and (c) Three-dimensional view

. The coordinate system is defined for the right arm with the person facing towards positive X (red arrow).

coupling between two different joint angles, but is currently only applied to 1-dimensional models [30]. An additional approach involved the application of machine learning to investigate biarticular muscle models, as demonstrated in the work by Nasr and McPhee [31]. However, this learning-based method necessitated a substantial volume of data. A previous approach applied two perpendicular single-DoF MTGs that were scaled using a torque ratio term [7]. Another approach implemented a 2-DoFs MTG by interpolating between experimental shoulder torques using a piecewise cubic Hermite polynomial by Nasr et al [11]. However, the impact of coupling between the 2-DoFs of the joint was not fully evaluated. Therefore, the goal of this research was to develop, for the first time, an MTG that accounts for the coupling between 2-DoFs of the shoulder joint. The shoulder joint was selected as it has multiple-DoFs and torques generated from multiple muscles with different lines of action [32–34]. The model aims to simplify the complexity of the shoulder joint for dynamic simulation purposes.

Three different forms of the 2-DoFs MTG model were designed with different degrees of coupling between DoFs, and biomechanical torque data was gathered to identify the scaling function parameters in the models. General models were fit to the experimental data for the three different coupling methods. The ability to predict joint torque was evaluated against experimental torques, leading to a comparison of degrees of coupling and model accuracy.

2 Material and Methods

2.1 Model Angle and Torque Definitions. The multi-DoFs MTG model aims to capture the coupling between two motions of the shoulder: shoulder plane of elevation (horizontal abduction/adduction), and shoulder elevation (flexion/extension) as defined according to the International Society of Biomechanics (ISB) [35]. Clinically, the shoulder plane of elevation is defined as horizontal adduction when the humerus moves horizontally across and towards the chest and is defined as horizontal abduction when it moves horizontally away from the chest [36]. Shoulder elevation is clinically defined as abduction when the plane of elevation is 0 ° and forward flexion when the plane of elevation is 90 ° [35].

Two angles were defined to describe these two motions:

- θ_1 = the angle of the plane of elevation of the humerus relative to the thorax (horizontal abduction/adduction);
- θ_2 = the angle of elevation of the humerus relative to the thorax (flexion/extension).

Figure 1 depicts the coordinate system and angle definitions. The coordinate system is defined using the ISB standards and is for the right arm with the person facing towards X.

Two torques were defined. The first torque, $\vec{\tau}_1$, is responsible for shoulder plane of elevation and is about Y in the direction of θ_1. The second torque, $\vec{\tau}_2$, is responsible for elevation and is about x' in the direction of θ_2. This second rotation results in elevation in the plane of elevation. Each torque is individually determined by considering the coupling between the DoFs. The resultant torque, $\vec{\tau}$, is at an angle α from the vertical (see Figure 1(c)).

The shoulder joint has a large Range of Motion (RoM) [33], ranging from 0 to 140 ° in horizontal adduction (θ_1 when θ_2 is 90 °) and 0 to 167 ° in forward flexion (θ_2 when θ_1 is 90 °) on average [37]. In this work, the model was defined to be for lifting and reaching motions such that θ_1 was defined to be between 0 and 120 ° and θ_2 between 60 and 160 °.

2.2 Coupling and MTG Equations. To develop the MTG functional forms for the torque magnitudes τ_1 and τ_2, the single-DoF MTG equation in Equation (1) was used. Models were developed to consider implicit coupling between the DoFs (**Model 1**), position coupling (**Model 2**), and position and velocity coupling (**Model 3**). In all models, the dependence of τ_p on ω was ignored because the slow speeds of reaching motions have a negligible impact [26].

Model 1 : Implicit Coupling

For implicit coupling, multiple single-DoF models were developed across the range of the secondary DoF. For τ_1, the torque-angle scaling and passive functions were determined with respect to θ_1 when θ_2 was 60, 85, 110, 135, and 160 °, and the torque-velocity scaling was determined with respect to $\dot{\theta}_1$ when $\dot{\theta}_2$ was 0 °/s. For τ_1, the torque-angle scaling and passive functions were determined with respect to θ_2 when θ_1 was 0, 30, 60, 90, and 120 °, and the torque-velocity scaling was determined with respect to $\dot{\theta}_2$ when $\dot{\theta}_1$ was 0 °/s. Linear interpolation between the curve fits was used to determine the torque scaling at points between the discrete values of θ_1 and θ_2. The implicit coupling equations for τ_1 and τ_2 are Equations (2) and (3), respectively. The subscript after the MTG function type indicates whether the function is for τ_1 or τ_2.

$$\tau_1 = \tau_{act_1} \cdot \tau_{\omega_1}(\dot{\theta}_1) \cdot \tau_{\theta_1}(\theta_1) + \tau_{p_1}(\theta_1)$$
$$\text{for } \theta_2 = 60, 85, 110, 135, 160\ ° \quad (2)$$

$$\tau_2 = \tau_{act_2} \cdot \tau_{\omega_2}(\dot{\theta}_2) \cdot \tau_{\theta_2}(\theta_2) + \tau_{p_2}(\theta_2)$$

(a) Isometric testing in elevation (b) Isometric testing in the plane of elevation (c) Isokinetic testing

Fig. 2 (a) Example of a participant setup when θ_1 is 0 ° and θ_2 is 85 ° for isometric testing in elevation. (b) Example of a participant setup when θ_1 is 0 ° and θ_2 is 85 ° for isometric testing in the plane of elevation. (c) Example of a participant setup for isokinetic testing where $\dot{\theta}_1$ was limited to 2.5 °/s and $\dot{\theta}_2$ 4.3 °/s for the trial.

$$\text{for } \theta_1 = 0, 30, 60, 90, 120\ ^\circ \quad (3)$$

Model 2 : Position Coupling

Next, the position coupling cases were developed such that the torque-angle scaling and passive functions were dependent on two angles, while the torque-velocity scaling function was dependent on one angular velocity as in the implicit coupling method. Equations (4) and (5) describe the position coupling MTG for both torques.

$$\tau_1 = \tau_{act_1} \cdot \tau_{\omega_1}(\dot{\theta_1}) \cdot \tau_{\theta_1}(\theta_1, \theta_2) + \tau_{p_1}(\theta_1, \theta_2) \quad (4)$$

$$\tau_2 = \tau_{act_2} \cdot \tau_{\omega_2}(\dot{\theta_2}) \cdot \tau_{\theta_2}(\theta_1, \theta_2) + \tau_{p_2}(\theta_1, \theta_2) \quad (5)$$

Model 3 : Position and Velocity Coupling

Finally, an additional degree of coupling was added to the torque-velocity scaling function such that it is dependent on two angular velocities instead of one. The coupled torque-angle scaling and the passive functions remain the same as **Model 2**. Equations (6) and (7) describe the position and velocity coupling MTG for τ_1 and τ_2, respectively.

$$\tau_1 = \tau_{act_1} \cdot \tau_{\omega_1}(\dot{\theta_1}, \dot{\theta_2}) \cdot \tau_{\theta_1}(\theta_1, \theta_2) + \tau_{p_1}(\theta_1, \theta_2) \quad (6)$$

$$\tau_2 = \tau_{act_2} \cdot \tau_{\omega_2}(\dot{\theta_1}, \dot{\theta_2}) \cdot \tau_{\theta_2}(\theta_1, \theta_2) + \tau_{p_2}(\theta_1, \theta_2) \quad (7)$$

For the three models, torque-angle scaling, torque-velocity scaling, and passive functions were developed. Polynomial torque-angle, and piecewise torque-velocity scaling functions have previously been found to be simple and effective functions for MTGs [18,20]. As the RoM evaluated was within the RoM of the shoulder, passive torques were expected to vary gradually as opposed to increasing exponentially outside the RoM [26]. Therefore, polynomial curves and surfaces were applied for all the scaling and passive relationships. To avoid over-fitting the data, curve and surface fits were evaluated to at most the third degree. For notation, curves are denoted as m-Curve, where m is the order of the polynomial curve and surfaces are denoted as m, n-Surface where m and n are the degree of the first and second independent variables.

Finally, an activation term approach similar to previous works was applied [5,15,20], where the activation torque, τ_{act}, is the product of an activation term (a_1 and a_2 for the plane of elevation and elevation, respectively) and the isometric torque, τ_{max}. The activation function for τ_1 or τ_2 is shown by Equation (8).

$$\tau_{act_{1,2}} = \tau_{max_{1,2}} a_{1,2} \quad (8)$$

where the activations are assumed to be:

$$a_1 = \cos(\alpha) \quad (9)$$

$$a_2 = \sin(\alpha) \quad (10)$$

The activations were assumed to be related to the resultant torque direction, α, where the activations are defined by Equations (9) and (10). This approach was inspired by vector addition as the magnitude of the two activations will always equate to 1 for maximal effort.

2.3 Shoulder Experiments. Isometric, isokinetic, and passive tests were conducted using the Biodex System 4 Pro (Biodex Medical Systems, Inc, Shirley, NY) which has a sampling rate of 100 Hz. All participants were instructed to keep their back against the seat and were secured using two straps. Participants were also instructed to keep their elbow and wrist joints locked in a neutral and straight position. The Biodex crank angle measurement was utilized as the shoulder angle, consistent with the approach taken by Brown and McPhee [20] in previous Biodex testing. To assess potential discrepancies between the Biodex crank angle measurement and the actual angle of the elbow joint, an electrogoniometer was employed in this study. The investigation revealed that the Biodex crank angle served as a close representation of the elbow joint angle, likely attributed to the rigid handle connecting the individual and the Biodex. These findings support the assumption that the crank angle aligns with the joint angle, ensuring the validity of our approach. The eligibility criteria of the study ensured that participants had not experienced any pain during activities of daily living within the past 6 months, and that the participant did not have any shoulder pain or an existing heart condition. Ethics approval was obtained from the University of Waterloo Research Ethics Board.

Isometric torque was measured in elevation for 25 different combinations of θ_1 ($0 \leq \theta_1 \leq 120\ ^\circ$) and θ_2 ($60 \leq \theta_2 \leq 160\ ^\circ$) evenly spread across the listed ranges. 10 males (24 ± 4 years, 1.79 ± 0.08 m, 78.2 ± 7.6 kg) and 10 females (22 ± 7 years, 1.63 ± 0.06 m, 59.6 ± 8.2 kg) participated in the study. Participants were instructed to use their Maximum Voluntary Contraction (MVC) for 5 seconds. Five passive tests were also done in elevation at 5 °/s, measuring the RoM of θ_2 for θ_1 at 0, 30, 60, 90, and 120 °. 20 concentric and 20 eccentric isokinetic combinations of $\dot{\theta_1}$ and $\dot{\theta_2}$ were measured using the MVC of the 20 participants ($-45 \leq \dot{\theta_1} \leq 45$ °/s, $-45 \leq \dot{\theta_2} \leq 45$ °/s).

Isometric torque was measured in the plane of elevation for 25 different combinations of θ_1 ($0 \leq \theta_1 \leq 120\ ^\circ$) and θ_2 ($60 \leq \theta_2 \leq 160\ ^\circ$). 7 male (26 ± 3 years, 1.80 ± 0.07 m, 79.0 ± 7.7 kg) and 6 female (24 ± 6 years, 1.63 ± 0.07 m, 59.5 ± 6.3 kg) subjects who

participated in the first study returned to participate. Five passive tests were done for plane of elevation torques at 5 °/s, measuring the RoM of θ_1 for θ_2 at 60, 85, 110, 135, and 160 °. Figure 2 shows an example of the Biodex setup for the two isometric and the isokinetic tests.

2.4 Data Processing. A 6 Hz low-pass 2nd-order Butterworth filter (6 Hz corner and 36 Hz cut-off frequency) was applied to all torque data to remove noise [38] according to our slow movements and inherent noise level of the device. The isometric torques were determined by selecting the highest average torque over 0.5 second intervals, as done in [39] and were normalized by an individual's maximum isometric torque. The isokinetic torques were found by regressing the maximum torque values against the average torque values to create a maximal dataset as described in [23]. For **Model 1** and **Model 2** without velocity coupling, the isokinetic torques were normalized by the maximum isometric torque. For **Model 3** with velocity coupling, the components of the maximum total torque cannot be divided by the maximum isometric torque as the muscle activation may not be maximum for the combination of $\dot{\theta_1}$ and $\dot{\theta_2}$, resulting in an unfair comparison between torques gathered purely in $\dot{\theta_1}$ or $\dot{\theta_2}$.The torque for an isokinetic test can be described as Equation (11).

$$\tau(\omega) = \tau_{act} \cdot \tau_{\omega}(\omega) \tag{11}$$

The measured torque, $\tau(\omega)$, can be divided by the activation torque, τ_{act}, to give the torque-velocity scaling function, $\tau_{\omega}(\omega)$, essentially normalizing the component isokinetic torques by the activation and the maximum isometric torque, allowing for a fair comparison.

The passive torques were then analysed by removing the contribution of gravitational torques. No normalization was required as the passive torques are not dependent on strength but instead on the passive structures in the shoulder.

2.5 Model Parameter Identification. In total, 32 best curves and surface fits were found for the torque-angle scaling, torque-velocity scaling, and passive functions for the three coupling models. A linear least squares method was used to find the polynomial curve or surface that best fit the experimental data for a given function. For the torque-velocity scaling functions, an additional constraint was added to ensure that the curves and surfaces had an intercept at one when the angular velocity was equal to zero, as done in previous torque-velocity scaling models [18,19,23]. An example of the constraint can be seen in Figure 3, where the concentric and eccentric curves meet at the intercept of 1. To determine the best fitting curve or surface, k-fold cross-validation with a k-value of 10 was used. The Root Mean Square Percent Error (RMSPE) of the 10-folds was determined with the best fit being the curve or surface with the lowest error. An example of a surface fit for the torque-angle scaling function can be seen in Figure 4.

2.6 Model Validation. The models were validated using isokinetic testing data where the angle and velocity dependencies were maintained. The isokinetic test was conducted at 5 °/s at an angle corresponding to an α of 60 °. The best curve and surface fits were found for the 2-DoFs MTG models; the shoulder joint angles (θ_1, θ_2) and the shoulder joint angular velocities ($\dot{\theta_1}$, $\dot{\theta_2}$) from the resulting experimental motion were the inputs of the models. Participant data was averaged for the isokinetic motion and the average experimental torque was compared against the model results.

3 Results

3.1 Model Parameter Identification. The curve and surface fit results for the three models are displayed in Table 1. The passive torques were normalized by the absolute maximum passive torque for comparison. The absolute maximum passive torques for τ_1 and τ_2 were 8.2 Nm and 4.3 Nm, respectively.

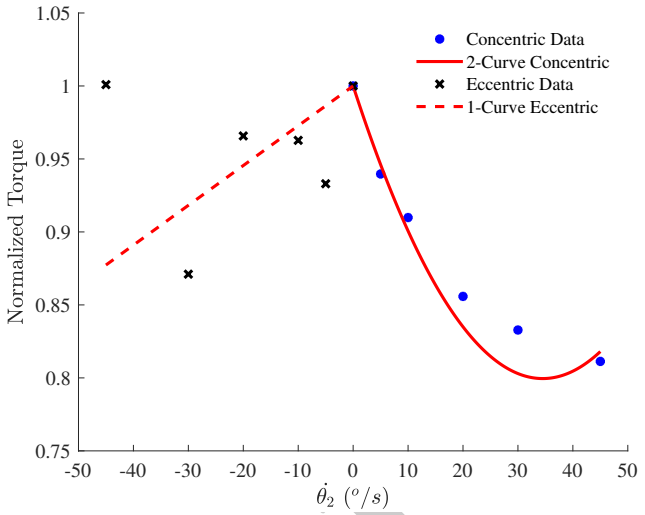

Fig. 3 Example of a piecewise torque-velocity scaling function curve fit with an intercept constraint at 1 when $\dot{\theta_2}$ = 0. The solid line in red represents a second-degree curve fit to the concentric data. The dashed red line represents the linear fit for the eccentric data.

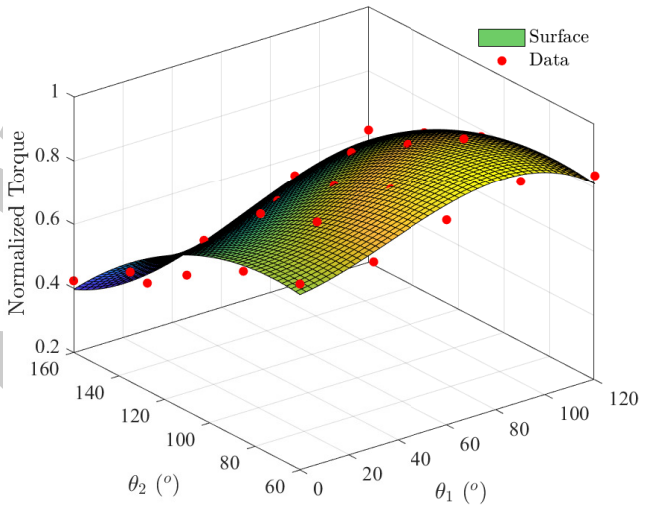

Fig. 4 Example of a surface fit used for the torque-angle scaling function. A 3, 2-Surface was found to be the best fit for the experimental data.

For the torque-angle scaling function, a 3-Curve is the best fit for $\tau_{\theta_1}(\theta_1)$ and a 2-Curve for $\tau_{\theta_2}(\theta_2)$. The cubic and quadratic relationship is also reflected in $\tau_{\theta_1}(\theta_1, \theta_2)$ and $\tau_{\theta_2}(\theta_1, \theta_2)$. The curve fits result in lower RMSPEs compared to the surface fits for the respective torque-angle scaling functions.

For the torque-velocity scaling functions, there is more variability in fit types. For $\tau_{\omega_1}(\dot{\theta_1})$, a cubic relationship was determined for both concentric and eccentric motions. For $\tau_{\omega_1}(\dot{\theta_1}, \dot{\theta_2})$, less of a trend is displayed, with a 1, 2-Surface being the best fit for concentric motions and a 2, 1-Surface for eccentric. For $\tau_{\omega_2}(\dot{\theta_1}, \dot{\theta_2})$, a 3, 2-Surface and a 3, 1-Surface were the best for concentric and eccentric motions, respectively. A higher RMSPE curves and surfaces fit to eccentric elevation data was observed compared to concentric elevation data. A higher RMSPE is also observed for the coupled surfaces compared to the respective curve fits.

For the passive torque functions, large RMSPEs are observed compared to the torque-angle and torque-velocity scaling functions. As the passive torques are low in the RoM studied, small

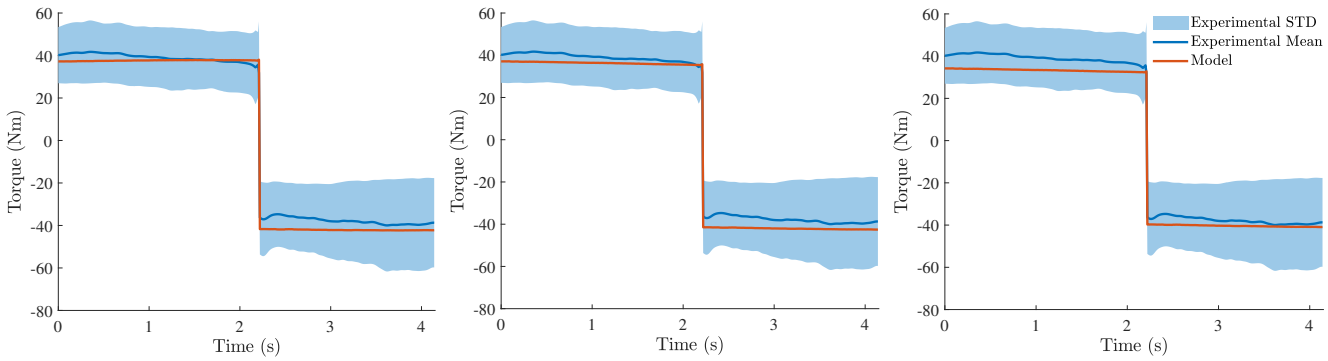

(a) Model 1 (b) Model 2 (c) Model 3

Fig. 5 Torque results for (a) Model 1, (b) Model 2, and (c) Model 3 compared against experimental torque data averaged across all participants. The standard deviation of the experimental data is also depicted.

Table 1 MTG functions fitting results and accuracy.

Function	Fit Type	RMSPE (%)
$\tau_{\theta_1}(\theta_1)$	3-Curve	14.0
$\tau_{\theta_2}(\theta_2)$	2-Curve	9.3
$\tau_{p_1}(\theta_1)$	3-Curve	36.4
$\tau_{p_2}(\theta_2)$	3-Curve	47.9
$\tau_{\omega_1}(\dot{\theta_1})$ Concentric	3-Curve	23.3
$\tau_{\omega_1}(\dot{\theta_1})$ Eccentric	3-Curve	20.9
$\tau_{\omega_2}(\dot{\theta_2})$ Concentric	2-Curve	10.5
$\tau_{\omega_2}(\dot{\theta_2})$ Eccentric	1-Curve	17.5
$\tau_{\theta_1}(\theta_1, \theta_2)$	3, 2-Surface	14.7
$\tau_{\theta_2}(\theta_1, \theta_2)$	3, 2-Surface	10.3
$\tau_{p_1}(\theta_1, \theta_2)$	3, 2-Surface	38.7
$\tau_{p_2}(\theta_1, \theta_2)$	2, 3-Surface	50.6
$\tau_{\omega_1}(\dot{\theta_1}, \dot{\theta_2})$ Concentric	1, 2-Surface	28.9
$\tau_{\omega_1}(\dot{\theta_1}, \dot{\theta_2})$ Eccentric	2, 1-Surface	26.0
$\tau_{\omega_2}(\dot{\theta_1}, \dot{\theta_2})$ Concentric	3, 2-Surface	19.7
$\tau_{\omega_2}(\dot{\theta_1}, \dot{\theta_2})$ Eccentric	3, 1-Surface	26.1

Table 2 Model validation results for total torque.

Model	RMSE (Nm)	RMSPE (%)
Model 1	3.5	8.5
Model 2	3.8	9.0
Model 3	4.7	11.3

errors have a greater effect on the RMSPE compared to isometric and isokinetic measurements. For $\tau_{p_1}(\theta_1)$ and $\tau_{p_2}(\theta_2)$, 3-Curves were the best fit. For $\tau_{p_1}(\theta_1, \theta_2)$ a 3, 2-Surface was the best fit. The cubic relationship results in an increase in passive torque towards the extreme RoMs, similar to that of the double exponential function commonly used for the passive scaling function.

3.2 Model validation. Table 2 presents the validation results for total torque using the three different coupling methods. The Root Mean Square Error (RMSE) and the RMSPE increased with an increase in the coupling, with **Model 3** resulting in the highest error. The increased validation error with an increase in coupling is consistent with the higher fitting errors observed in MTG functions with coupling (Table 1). The average and standard deviation of the experimental data for the torque predicted by the models have been plotted to compare the errors in Figure 5.

In Figure 5 the first half of the motion is concentric, and the second half is eccentric (resulting in negative torques). **Model 1** shows the best estimation for concentric motion, with a slight overestimation of eccentric torques. **Model 2** resulted in a slight underestimation of the torque in concentric motion. **Model 3** introduces the coupled torque-velocity scaling functions ($\tau_{\omega_1}(\dot{\theta_1}, \dot{\theta_2})$ and $\tau_{\omega_2}(\dot{\theta_1}, \dot{\theta_2})$). In concentric motions, the impact of the coupled torque-velocity scaling function results in an underestimation of the torque. However, in eccentric motions the coupled torque-velocity scaling performs better than the uncoupled torque-velocity scaling, reducing the overestimation of the eccentric torques.

4 Discussion

The study presented a new 2-DoFs MTG that models torque data as a function of two angles and two angular velocities. **Model 1**, which used single-DoF curves at discrete intervals with linear interpolation between, resulted in the lowest RMSE of 3.5 Nm (8.5%) and is the recommended approach. The accuracy of **Model 1** could be attributed to the single-DoF torque-angle and torque-velocity scaling functions of **Model 1** ($\tau_{\theta_1}(\theta_1)$, $\tau_{\theta_2}(\theta_2)$, $\tau_{\omega_1}(\dot{\theta_1})$, and $\tau_{\omega_1}(\dot{\theta_2})$) resulting in the lower fitting errors compared to their coupled counterparts ($\tau_{\theta_1}(\theta_1, \theta_2)$, $\tau_{\theta_2}(\theta_1, \theta_2)$, $\tau_{\omega_1}(\dot{\theta_1}, \dot{\theta_2})$, and $\tau_{\omega_1}(\dot{\theta_1}, \dot{\theta_2})$). As the test population has differences in shoulder anatomy, it is difficult to accurately represent a group [40]. Therefore, it is simpler to fit a population trend for the five experimental measurements in a single-DoF compared to the 25 measurements of the coupled 2-DoFs.

Comparing the curve and surface fitting results, eccentric curve and surface fits had higher fitting errors compared to concentric fits for elevation torques (τ_2). Participants indicated that the eccentric motions were more tiring, and it is likely that not all participants used their MVC as discussed in the work of Yeadon et al [23]. This led to wide-spread eccentric torque data that did not increase above the concentric torque, resulting in a lower torque compared to previous model predictions [6,18,19]. The variation in eccentric torques can also be observed in Fig 5, where the eccentric torques have a larger standard deviation compared to the concentric. Higher fitting errors were also more commonly observed in the torque-velocity scaling fits compared to the torque-angle scaling fits. The higher errors could be due to the intercept constraint that was used to avoid discontinuity between concentric and eccentric curves, along with the fact that participants found the isokinetic testing more tiring compared to isometric testing. The passive torque fitting errors were also significantly larger than the other MTG functions. However, the passive torques are significantly smaller than the active torques and therefore the model errors are minimally affected by the passive torques.

A limitation of the study is the constraint imposed on the model's motions and speed, which have been limited to lifting and reaching activities. Consequently, the model is not intended for high-speed sporting applications. Another limitation is the sine and cosine

activation relationship assumed in Equations (9) and (10). It is possible that the activations calculated for the models do not accurately represent the muscle activations of the population. It has also previously been shown that there are differences in how women and men activate their shoulder muscles under isometric loading, with women typically showing a lower muscle activation in muscles that act in the primary force direction and more activation in other muscles [41]. Therefore, it would be beneficial to consider different activation approaches, as well as sex-specific models in the future.

Future work could enhance model validation by incorporating additional experimental testing, and considering the impact of biarticular muscles on the model. In future directions, consideration may be given to incorporate statistical parametric mapping analysis [42] as an alternative method for assessing differences between experimental and simulated curves. The application of statistical parametric mapping could offer insights into the nuanced variations across multiple participants, providing a more comprehensive understanding of the model's performance.

As demonstrated in the machine learning study [31], one potential and effective approach involves the use of surface electromyography signals to create associations with the activation of biarticular muscles. These correlations should be bidirectional, encompassing both electromyography signals and muscle activation, as emphasized in related studies [4,43], with a specific focus on biarticular muscles.

An alternative approach to mitigate over-fitting involves exploring a weighting method during the fitting process, ensuring that all data points are positioned beneath the curve. This method enhances the model's generalization by assigning appropriate significance to each data point, thereby contributing to a more robust and representative fit.

5 Conclusions

Work in the field of muscle modeling has led to the innovation of MTGs, a model that reduces the complexity of muscle-force models to a single torque at the joint, allowing for faster dynamic simulations. However, there is a lack of MTG models that account for coupling between 2-DoFs at a joint, leading to complexity in modeling three-dimensional motion for complicated joints such as the shoulder. This motivated the development of a multi-DoFs MTG as a function of two angles and angular velocities at the shoulder joint. The research was completed with the development of a general 2-DoFs MTG model for the different degrees of coupling for the first time, comparing the effect that coupling has on the model accuracy.

Acknowledgment

This research was supported by funding from the Natural Sciences and Engineering Research Council of Canada and the University of Waterloo.

Funding Data

- The Natural Sciences and Engineering research Council of Canada (*Discovery Grant*)
- The University of Waterloo Engineering Excellence Fellowship

Authors' Contributions

Methodology, experiments, and writing the first draft S.B.; A.N. visualization; editing S.B., A.N., and J.M.; conceptualization, and funding acquisition J.M.; All authors have read and agreed to the published version of the manuscript.

Institutional review board statement

The study was conducted according to the guidelines of the Declaration of Helsinki, and approved by the Office of Research Ethics of the University of Waterloo #44157.

Data availability statement

The data generated and/or analyzed during the current study are not publicly available for legal/ethical reasons but are available from the corresponding author on reasonable request.

Abbreviations

DoF Degree of Freedom.

ISB International Society of Biomechanics.

MTG Muscle Torque Generator.

MVC Maximum Voluntary Contraction.

RMSE Root Mean Square Error.

RMSPE Root Mean Square Percent Error.

RoM Range of Motion.

Nomenclature

a = time-varying muscle activation term for an arbitrary MTG
a_1 = muscle activation term for the plane of elevation
a_2 = muscle activation term for elevation

Greek Letters

α = the direction of the resultant torque (°)
θ = joint angle for an arbitrary single-DoF MTG (°)
θ_1 = angle describing the plane of elevation of the humerus relative to the thorax (°)
θ_2 = angle describing elevation of the humerus relative to the thorax (°)
$\dot{\theta}_1$ = angular velocity describing the rate of change of the plane of elevation of the humerus relative to the thorax (°/s)
$\dot{\theta}_2$ = angular velocity describing the rate of change of elevation of the humerus relative to the thorax (°/s)
$\vec{\tau}$ = resultant torque in the direction of α (Nm)
$\vec{\tau}_1$ = torque responsible for shoulder plane of elevation in the direction of θ_1 (Nm)
$\vec{\tau}_2$ = torque responsible for shoulder elevation in the direction of θ_2 (Nm)
τ_{act} = scalar activation torque of an MTG (Nm)
τ_{max} = maximum allowed isometric torque for an MTG (Nm)
τ_p = passive torque function of an MTG (Nm)
τ_θ = torque-angle scaling function of an MTG
τ_ω = torque-velocity scaling function of an MTG
ω = joint angular velocity for an arbitrary single-DoF MTG (°/s)

References

[1] Febrer-Nafría, M., Nasr, A., Ezati, M., Brown, P., Font-Llagunes, J. M., McPhee, J. (2022) Predictive multibody dynamic simulation of human neuromusculoskeletal systems: A review. *Multibody System Dynamics* pp 1–41. doi: 10.1007/s11044-022-09852-x

[2] Ghannadi, B., Razavian, R. S., McPhee, J. (2018) Upper extremity rehabilitation robots: A survey. In: Handbook of Biomechatronics. Elsevier, San Diego, CA, USA, chap 9, p 319–353, doi: 10.1016/B978-0-12-812539-7.00012-X

[3] Nasr, A., Hunter, J., Dickerson, C. R., McPhee, J. (2023) Evaluation of a machine learning-driven active-passive upper limb exoskeleton robot: Experimental human-in-the-loop study. *Wearable Technologies* 4:e13. doi: 10.1017/wtc.2023.9

[4] Nasr, A., Bell, S., He, J., Whittaker, R. L., Jiang, N., Dickerson, C. R., McPhee, J. (2021) MuscleNET: Mapping electromyography to kinematic and dynamic biomechanical variables. *Journal of Neural Engineering* 18(4):0460d3. doi: 10.1088/1741-2552/ac1adc

[5] Jansen, C., McPhee, J. (2020) Predictive dynamic simulation of Olympic track cycling standing start using direct collocation optimal control. *Multibody System Dynamics* 49(1):53–70. doi: 10.1007/s11044-020-09723-3

[6] MacKenzie, S. J., Sprigings, E. J. (2009) A three-dimensional forward dynamics model of the golf swing. *Sports Engineering* 11(4):165–175. doi: 10.1007/s12283-009-0020-9

[7] McNally, W., McPhee, J. (2018) Dynamic optimization of the golf swing using a six degree-of-freedom biomechanical model. In: Proceedings, vol 2. MDPI, Brisbane, Queensland, Australia, p 243, doi: 10.3390/proceedings2060243
[8] Archibald Vivian, H. (1979) The heat of shortening and the dynamic constants of muscle. *Proceedings of the Royal Society of London B: Biological Sciences* 205(1161):211–30
[9] Cleather, D. J., Bull, A. M. (2010) Lower-extremity musculoskeletal geometry affects the calculation of patellofemoral forces in vertical jumping and weightlifting. *Proceedings of the Institution of Mechanical Engineers, Part H: Journal of Engineering in Medicine* 224(9):1073–1083. doi: 10.1243/09544119JEIM731
[10] Sherman, M. A., Seth, A., Delp, S. L. (2013) What is a moment arm? Calculating muscle effectiveness in biomechanical models using generalized coordinates. In: Proceedings of the ASME Design Engineering Technical Conference, vol 7 B. ASME, Portland, Oregon, USA, doi: 10.1115/DETC2013-13633
[11] Nasr, A., Hashemi, A., McPhee, J. (2023) Scalable musculoskeletal model for dynamic simulations of upper body movement. *Computer Methods in Biomechanics and Biomedical Engineering* pp 1–32. doi: 10.1080/10255842.2023.2184747
[12] Nasr, A., McPhee, J. (2024) Scalable musculoskeletal model for dynamic simulations of lower body movement. *Computer Methods in Biomechanics and Biomedical Engineering* pp 1–27. doi: 10.1080/10255842.2024.2316240
[13] De Groote, F., Kinney, A. L., Rao, A. V., Fregly, B. J. (2016) Evaluation of direct collocation optimal control problem formulations for solving the muscle redundancy problem. *Annals of Biomedical Engineering* 44(10):2922–2936. doi: 10.1007/s10439-016-1591-9
[14] Inkol, K. A., Brown, C., McNally, W., Jansen, C., McPhee, J. (2020) Muscle torque generators in multibody dynamic simulations of optimal sports performance. *Multibody System Dynamics* 50(4):435–452. doi: 10.1007/s11044-020-09747-9
[15] Millard, M., Emonds, A. L., Harant, M., Mombaur, K. D. (2019) A reduced muscle model and planar musculoskeletal model fit for the simulation of whole-body movements. *Journal of Biomechanics* 89:11–20. doi: 10.1016/j.jbiomech.2019.04.004
[16] Kulig, K., Andrews, J. G., Hay, J. G. (1984) Human strength curves. *Exercise and Sport Sciences Reviews* 12(1):417–466. doi: 10.1249/00003677-198401000-00014
[17] Gordon, A. M., Huxley, A. F., Julian, F. J. (1966) The variation in isometric tension with sarcomere length in vertebrate muscle fibres. *The Journal of Physiology* 184(1):170–192. doi: 10.1113/jphysiol.1966.sp007909
[18] Haering, D., Pontonnier, C., Bideau, N., Nicolas, G., Dumont, G. (2019) Using torque-angle and torque-velocity models to characterize elbow mechanical function: Modeling and applied aspects. *Journal of Biomechanical Engineering* 141(8):084501. doi: 10.1115/1.4043447
[19] Anderson, D. E., Madigan, M. L., Nussbaum, M. A. (2007) Maximum voluntary joint torque as a function of joint angle and angular velocity: Model development and application to the lower limb. *Journal of Biomechanics* 40(14):3105–3113. doi: 10.1016/j.jbiomech.2007.03.022
[20] Brown, C., McPhee, J. (2020) Predictive forward dynamic simulation of manual wheelchair propulsion on a rolling dynamometer. *Journal of Biomechanical Engineering* 142(7):071008. doi: 10.1115/1.4046298
[21] Harry, J. D., Ward, A. W., Heglund, N. C., Morgan, D. L., McMahon, T. A. (1990) Cross-bridge cycling theories cannot explain high-speed lengthening behavior in frog muscle. *Biophysical Journal* 57(2):201–208. doi: 10.1016/S0006-3495(90)82523-6
[22] King, M. A., Yeadon, M. R. (2002) Determining subject-specific torque parameters for use in a torque-driven simulation model of dynamic jumping. *Journal of Applied Biomechanics* 18(3):207–217. doi: 10.1123/jab.18.3.207
[23] Yeadon, M. R., King, M. A., Wilson, C. (2006) Modelling the maximum voluntary joint torque/angular velocity relationship in human movement. *Journal of Biomechanics* 39(3):476–482. doi: 10.1016/j.jbiomech.2004.12.012
[24] Hoang, P. D., Gorman, R. B., Todd, G., Gandevia, S. C., Herbert, R. D. (2005) A new method for measuring passive length-tension properties of human gastrocnemius muscle in vivo. *Journal of Biomechanics* 38(6):1333–1341. doi: 10.1016/j.jbiomech.2004.05.046
[25] Riener, R., Edrich, T. (1999) Identification of passive elastic joint moments in the lower extremities. *Journal of Biomechanics* 32(5):539–544. doi: 10.1016/S0021-9290(99)00009-3
[26] Yamaguchi, G. T. (2006) *Dynamic modeling of musculoskeletal motion: A vectorized approach for biomechanical analysis in three dimensions*, 1st edn. Springer, Boston, MA, USA, doi: 10.1007/978-0-387-28750-8
[27] King, M. A., Wilson, C., Yeadon, M. R. (2006) Evaluation of a torque-driven model of jumping for height. *Journal of Applied Biomechanics* 22(4):264–274. doi: 10.1123/jab.22.4.264
[28] Suzuki, Y., Nomura, T., Casadio, M., Morasso, P. (2012) Intermittent control with ankle, hip, and mixed strategies during quiet standing: A theoretical proposal based on a double inverted pendulum model. *Journal of Theoretical Biology* 310:55–79. doi: 10.1016/j.jtbi.2012.06.019
[29] Forrester, S. E., Yeadon, M. R., King, M. A., Pain, M. T. (2011) Comparing different approaches for determining joint torque parameters from isovelocity dynamometer measurements. *Journal of Biomechanics* 44(5):955–961. doi: 10.1016/j.jbiomech.2010.11.024
[30] Lewis, M. G., Yeadon, M. R., King, M. A. (2021) Are torque-driven simulation models of human movement limited by an assumption of monoarticularity? *Applied Sciences* 11(9):3852. doi: 10.3390/app11093852
[31] Nasr, A., McPhee, J. (2022) Biarticular MuscleNET: A machine learning model of biarticular muscles. In: Proceedings of the North American Congress on Biomechanics, Ottawa, Canada
[32] McDonald, A. C., Savoie, S. M., Mulla, D. M., Keir, P. J. (2018) Dynamic and static shoulder strength relationship and predictive model. *Applied Ergonomics* 67:162–169. doi: 10.1016/j.apergo.2017.10.004
[33] Veeger, H. E., van der Helm, F. C. (2007) Shoulder function: The perfect compromise between mobility and stability. *Journal of Biomechanics* 40(10):2119–2129. doi: 10.1016/j.jbiomech.2006.10.016
[34] Nasr, A. (2022) Design, dynamics, and control of active-passive upper-limb exoskeleton robots. PhD thesis, University of Waterloo, Waterloo, ON, Canada
[35] Wu, G., Van Der Helm, F. C., Veeger, H. E., Makhsous, M., Van Roy, P., Anglin, C., Nagels, J., Karduna, A. R., McQuade, K., Wang, X., Werner, F. W., Buchholz, B. (2005) ISB recommendation on definitions of joint coordinate systems of various joints for the reporting of human joint motion - Part II: Shoulder, elbow, wrist and hand. *Journal of Biomechanics* 38(5):981–992. doi: 10.1016/j.jbiomech.2004.05.042
[36] Miniato, M. A., Caire, M. J. (2018) *Anatomy, Shoulder and Upper Limb, Shoulder*. StatPearls Publishing
[37] Namdari, S., Yagnik, G., Ebaugh, D. D., Nagda, S., Ramsey, M. L., Williams, G. R., Mehta, S. (2012) Defining functional shoulder range of motion for activities of daily living. *Journal of Shoulder and Elbow Surgery* 21(9):1177–1183. doi: 10.1016/j.jse.2011.07.032
[38] Chong, H. C., Tennant, L. M., Kingston, D. C., Acker, S. M. (2017) Knee joint moments during high flexion movements: Timing of peak moments and the effect of safety footwear. *Knee* 24(2):271–279. doi: 10.1016/j.knee.2016.12.006
[39] Pinter, I. J., Bobbert, M. F., van Soest, A. J., Smeets, J. B. (2010) Isometric torque-angle relationships of the elbow flexors and extensors in the transverse plane. *Journal of Electromyography and Kinesiology* 20(5):923–931. doi: 10.1016/j.jelekin.2010.05.001
[40] Dickerson, C. R., Hughes, R. E., Chaffin, D. B. (2008) Experimental evaluation of a computational shoulder musculoskeletal model. *Clinical Biomechanics* 23(7):886–894. doi: 10.1016/j.clinbiomech.2008.04.004
[41] Anders, C., Bretschneider, S., Bernsdorf, A., Erler, K., Schneider, W. (2004) Activation of shoulder muscles in healthy men and women under isometric conditions. *Journal of Electromyography and Kinesiology* 14(6):699–707. doi: 10.1016/j.jelekin.2004.04.003
[42] Giordano, K. A., Cich, M., Oliver, G. D. (2023) Length-tension differences between concentric and eccentric shoulder rotation strength. *Journal of Strength and Conditioning Research* pp 10–1519. doi: 10.1519/jsc.0000000000004625
[43] Nasr, A., Inkol, K. A., Bell, S., McPhee, J. (2021) InverseMuscleNET: Alternative machine learning solution to static optimization and inverse muscle modelling. *Frontiers in Computational Neuroscience* 15:759489. doi: 10.3389/fncom.2021.759489

Contents

List of Figures

List of Tables